**Supplementary Information**

Supplementary Text
De novo transcriptome assembly and reconstruction of metagenome-assembled genomes

De novo assembly of the transcripts independently confirmed that the SRB partners of ANME were inactive in the presence of AQDS. The majority of the expressed genes in the active conditions (Sulfate, AQDS, and AQDS+Sulfate) were associated with the *Methanosarcinales* (Supplementary Figure 6A), the order of which all families of ANME-2 belong [1]. Expressed genes associated with the *Deltaproteobacteria* (now known as the *Desulfobacterota* [2]), which harbor the dominant SRB lineage SEEP-SRB1 in our sediment sample, were a large portion of the total transcripts when sulfate was actively consumed as the electron acceptor for AOM, but significantly decreased in the AQDS or AQDS+Sulfate conditions (Supplementary Figure 6A). With the caveat that not all of the transcripts could be confidently assigned to order or class levels, our taxonomic analysis of the transcripts support that ANME and SRB are the most abundant active members in the seep sediment incubations. Assignment of mRNA transcripts to known metabolic pathways revealed the majority were assigned to methane metabolism, a pathway that was highly expressed in all conditions relative to the no electron acceptor control (Supplementary Figure 6B). Transcripts assigned to sulfur metabolism were abundant in the Sulfate condition, but significantly lower in AQDS, AQDS+Sulfate and no electron acceptor control (None) conditions (Supplementary Figure 6B).

We reconstructed metagenome-assembled genomes (MAGs) that represent the core genomes of the dominant ANME (ANME-2a and ANME-2c) and SRB lineages (SEEP-SRB1a and SEEP-SRB1g) from the high-coverage reads of bulk sediment metagenome of the same sediment sample used for the metatranscriptomics analysis (Supplementary Text, Supplementary Table 3). Given the inherent high strain-level heterogeneity among co-occurring ANME in seep sediments, the reconstructed MAGs are smaller than the expected genome size of 3-4 Mb based on previous studies [3–5] and likely represent the core rather than the variable component of the genome between strains. The SEEP-SRB1g MAG is notably smaller (only 0.6 Mb) and estimated at only 36% genome completeness, whereas the MAGs of ANME-2a, ANME-2c and SEEP-SRB1a estimated at ~ 90% genome completeness (Supplementary Table 3). Together, these 4 MAGs account for the majority of the transcripts under our experimental conditions, with the two ANMEs accounting for 62% and the two SRBs accounting for 16% of the non-rRNA transcripts on average recovered in the Sulfate condition (Supplementary Figure 7). Previous transcriptomic studies of AOM consortia also reported ANME accounting for a greater proportion of the expressed genes than SRB [4], which is in contrast to the presumed anabolic activity of ANME and SRB measured from nanoSIMS-based single cell ^{15}N-ammonium assimilation data (Figure 4). Compared to the no electron acceptor control condition, both ANME-2a and ANME-2c showed an upregulation in transcripts with the addition of either sulfate or AQDS as the electron acceptor, whereas SEEP-SRB1a and SEEP-SRB1g showed transcriptional upregulation in the Sulfate condition only (Figure 5).

Supplementary Tables and Figures

Supplementary Figure 1. Sediment microcosms incubated with N_2/CO_2 (80/20) and different electron acceptors. Activities of methane-oxidizing consortia were tracked by **A**, production of ^{13}C-dissolved inorganic carbon, **B**, concentration of sulfate, and **C**, concentration of reduced AQDS (AQH_2DS). One biological replicate was performed for each electron acceptor condition.
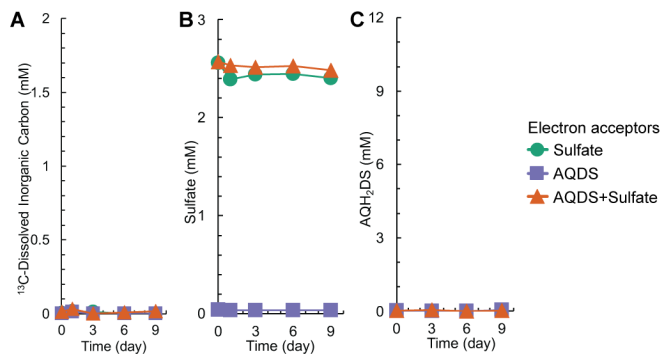
Supplementary Figure 2. Examples of paired phylogenetic identification and anabolic activity of AOM consortia with different electron acceptors revealed by FISH-nanoSIMS. **A,D,G,J**, FISH images of AOM consortia with ANME in red and SRB in green. Scale bar = 2 μm. **B,E,H,K**, Corresponding nanoSIMS ion images of $^{14}N^{12}C^-$ as a proxy for biomass, with bars showing ion counts on the right. **C,F,I,L**, Single cell activity shown as ^{15}N atom percentage in regions of interest (ROI). ANME ROIs are outlined in red and SRB ROIs are outlined in green. Assimilation of $^{15}NH_4^+$ into the biomass is used as a proxy for cellular anabolic activity, with bars showing ^{15}N atom percentages on the right.
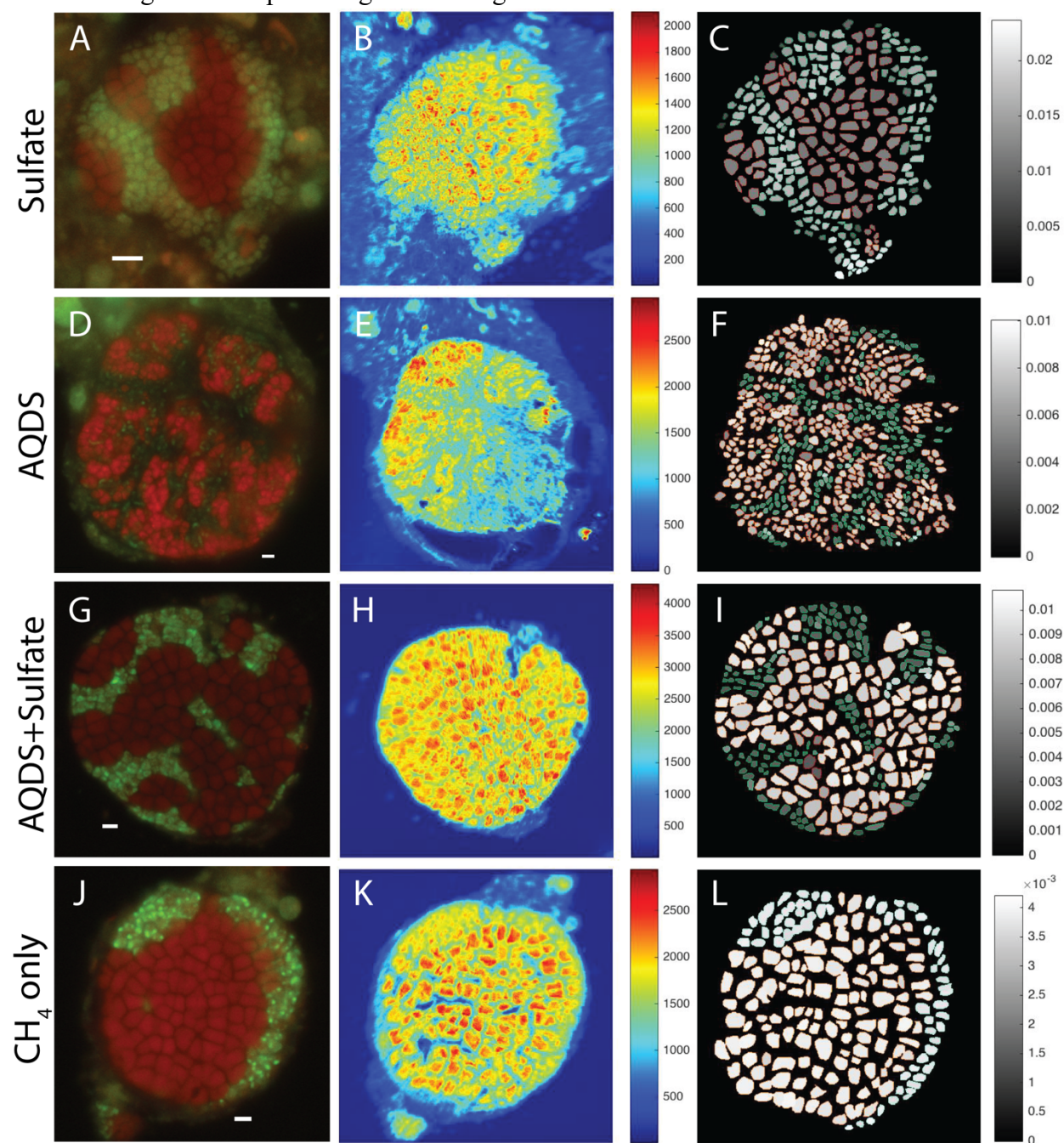
Supplementary Figure 3. Correlation of ANME-2 anabolic activity and catabolic activity after 9 days of incubation. The anabolic activity was measured by ^{15}N-ammonia incorporation into ANME-2a or ANME-2c consortia (Supplementary Table 5). The catabolic activity was measured by ^{13}C-dissolved inorganic carbon produced from [13]CH$_4$ oxidation (Figure 1).
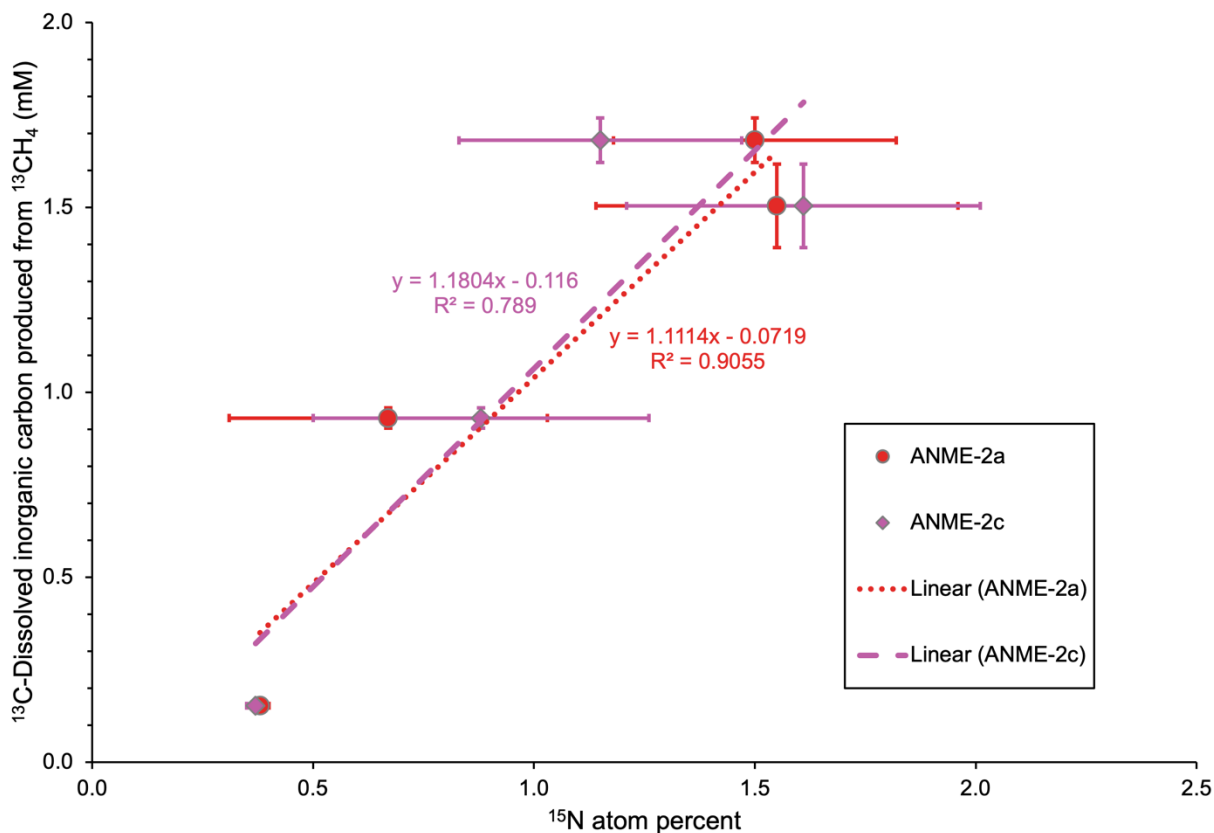
Supplementary Figure 4. Average relative sulfur content of ANME-2a and ANME-2c ($^{32}S/^{12}C^{14}N$ ANME) vs their syntrophic SRB partner ($^{32}S/^{12}C^{14}N$ SRB). ANME-SRB consortia with different electron acceptors under CH_4 were evaluated after 9 days of incubation. The sulfur content of ANME or SRB cells ($^{32}S/^{12}C^{14}N$) were similar in our active incubations as previously reported [6]. The sulfur content of ANME showed no significant difference to that of SRB in the same consortium in the 80 consortia analyzed (i.e. above or below the 1:1 line). The number of consortia analyzed in each electron acceptor condition can be found in Supplementary Table 5. Error bars represent standard deviation of the sulfur content of the cells in each consortium.
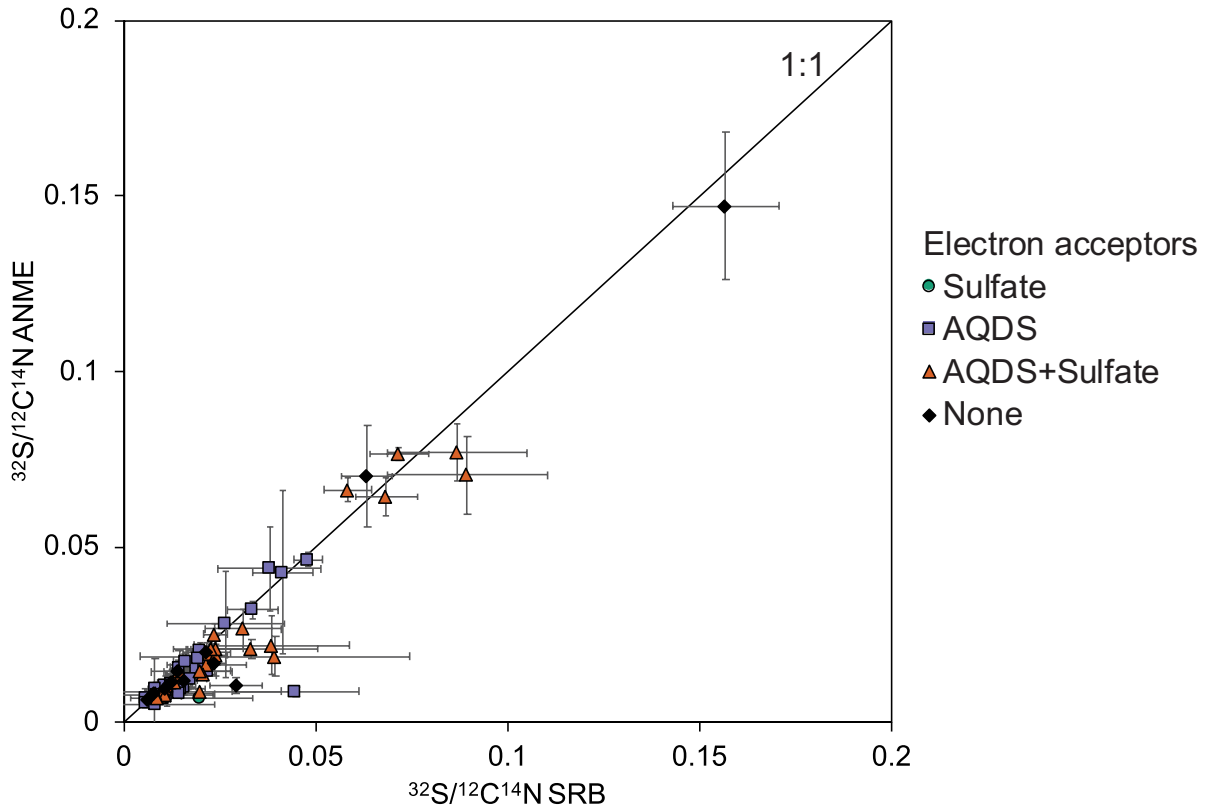
Supplementary Figure 5. The relationship between cell sulfur content and anabolism in $^{15}NH_4^+$ incubations with different electron acceptors for ANME-2a and ANME-2c cells. The cellular sulfur content ($^{32}S/^{12}C^{14}N$) of ANME-2a cell ROIs (n=2948) and ANME-2c cell ROIs (n=1225) were similar in our active incubations as previously reported [6]. However, in contrast to the previous report, no significant correlation was found between the cell sulfur content and anabolism, indicating that ANME is not turning over sulfur proportional to their anabolic activity (^{15}N-ammonium incorporation into the biomass). Cells are colored based on the consortium they are from. While a few consortia showed higher sulfur content than the rest, the sulfur content of the consortia in the presence and in the absence of AQDS were not significantly different (AQDS+Sulfate v.s. Sulfate: p= 0.19 for ANME-2a, p= 0.38 for ANME-2c; AQDS v.s. Sulfate: p=0.39 for ANME-2a, p=0.28 for ANME-2c; two-tailed t-test with equal variance). The number of cell ROIs analyzed in each electron acceptor condition can be found in Supplementary Table 4.
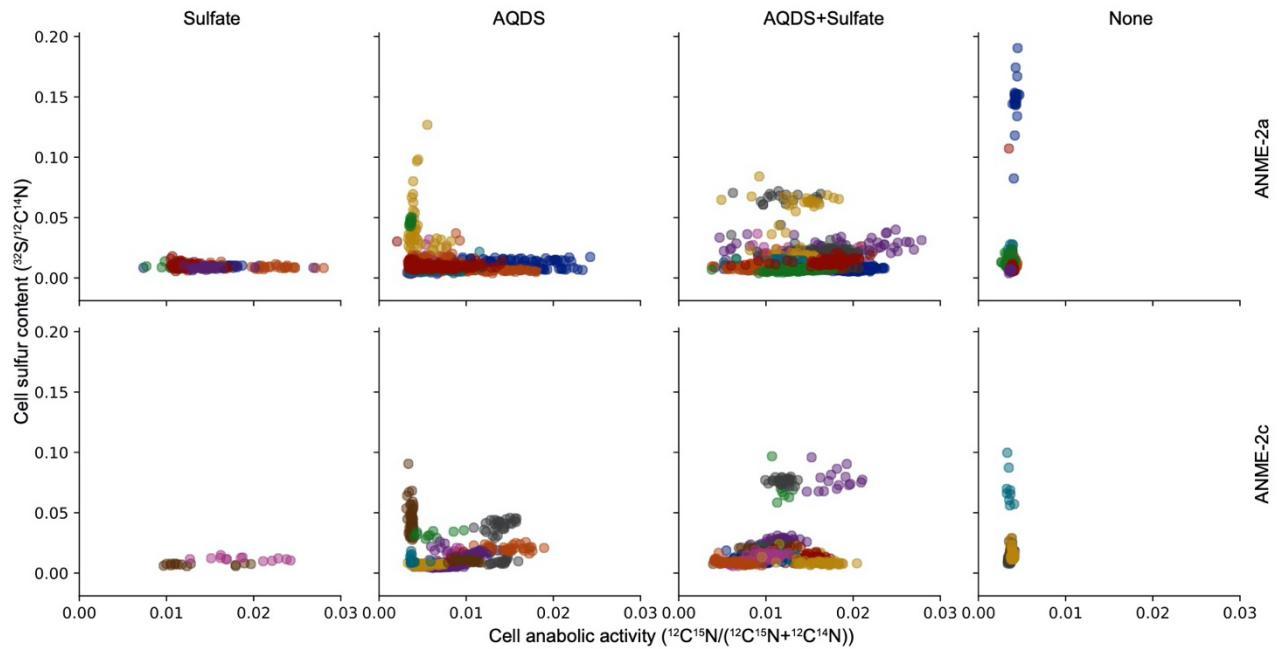
Supplementary Figure 6. Overview of metatranscriptome with different electron acceptors.
A, Taxonomy assignment of mRNA reads based on NCBI Refseq database. **B**, Major metabolic pathway assignment of mRNA reads based on KEGG database. Error bars represent standard deviations of triplicate day 9 samples.

A)
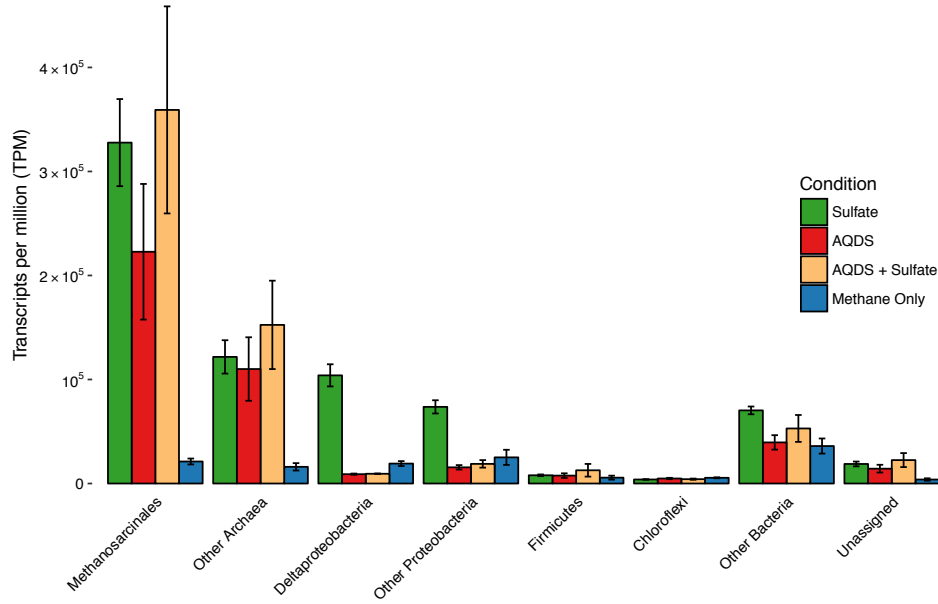
B)
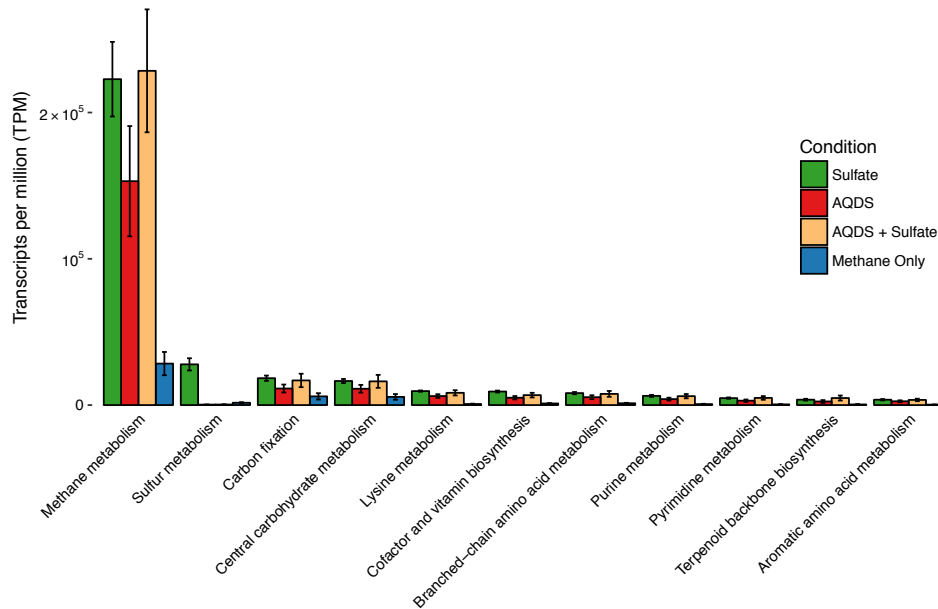
Supplementary Figure 7. Proportion of the non-rRNA transcripts accounted for by metagenome-assembled genomes from the bulk metagenome.
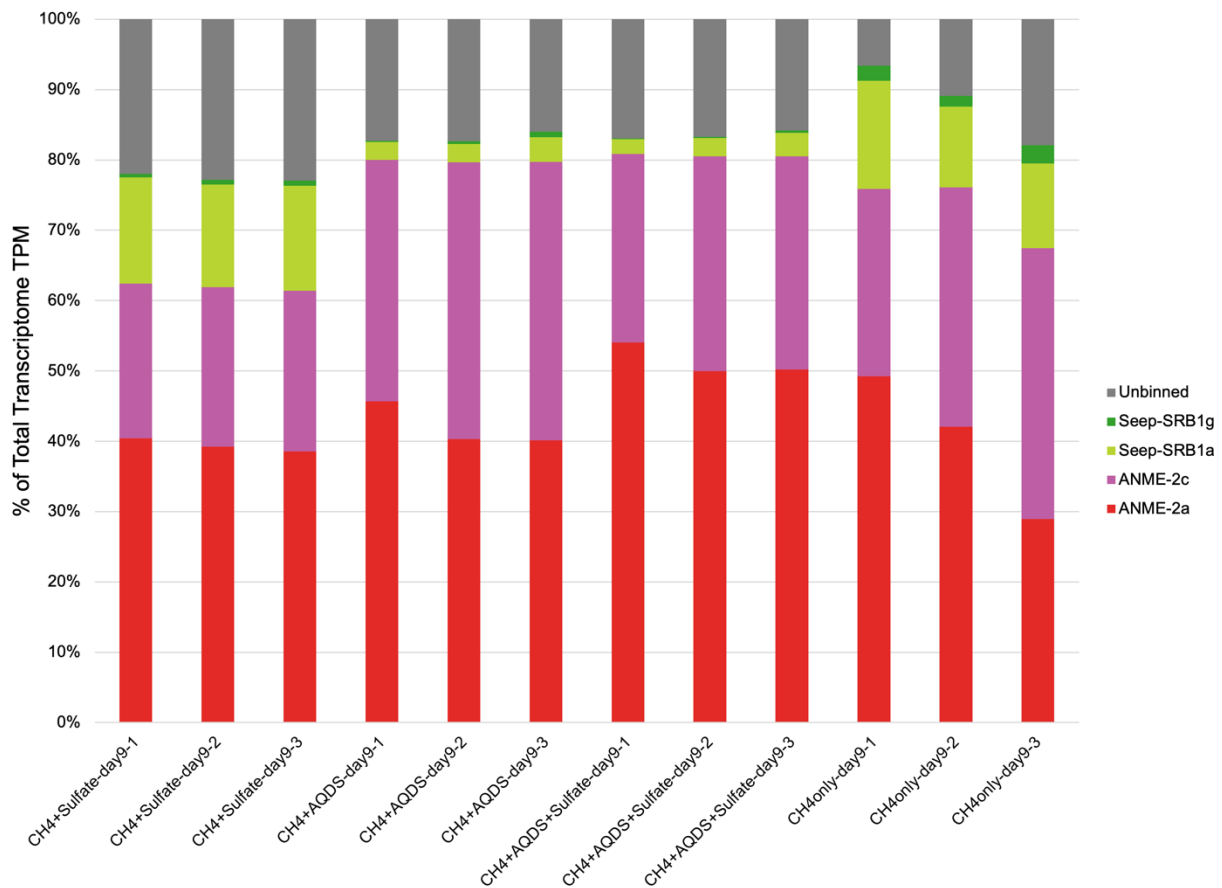
Supplementary Figure 8. Gene expression distributions of AOM consortia with different electron acceptors after 3 days of incubation. Normalized transcript per million (TPM) was used to compare RNA expression of ANME-2 and SEEP-SRB1 lineages based on their metagenome assembled genomes. Dashed lines indicate the quartiles of the distributions.
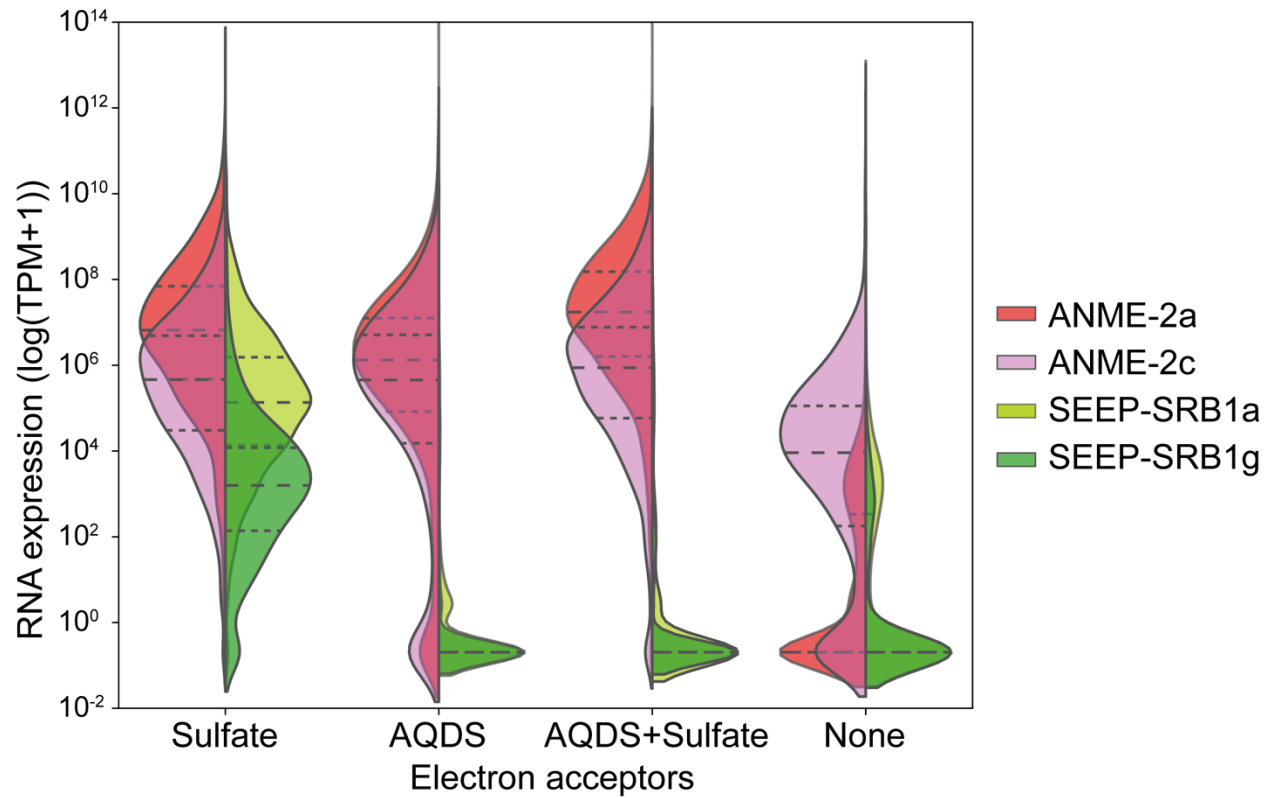
Supplementary Table 1. Summary of incubation sampling. A total of 45 seep sediment microcosms with different headspace gas and electron acceptors were setup on day 0. **A**, Supernatant from the replicated microcosms were sampled for geochemical measurements and the number of replicates used for each time point in the analysis is indicated in the table. **B**, The number of microcosms used for RNA analysis.

A

	day 0	day 3	day 6	day 9
CH$_4$+sulfate	1	10	5	3
CH$_4$+AQDS	1	10	6	3
CH$_4$+sulfate+AQDS	1	10	6	3
CH$_4$ only	1	8	5	3
N$_2$:CO$_2$+sulfate				1
N$_2$:CO$_2$+AQDS				1
N$_2$:CO$_2$+sulfate+AQDS				1

B

	day 3	day 9
CH$_4$+sulfate	1	3
CH$_4$+AQDS	1	3
CH$_4$+sulfate+AQDS	1	3
CH$_4$ only	1	3

Supplementary Table 2. Community composition analysis of sediment #7142 using iTag 16S rRNA amplicon sequencing.
(separate table)

Supplementary Table 3. Statistics of the bulk metagenome and metagenome-assembled genomes.

	Bulk metagenome	ANME-2 cluster archaeon S7142MS1 (ANME-2a)	ANME-2 cluster archaeon S7142MS2 (ANME-2c)	Desulfobacterales bacterium S7142MS3 (SEEP-SRB1a)	Desulfobacterales bacterium S7142MS4 (SEEP-SRB1g)
Genome size (bp)		1813034	1647749	2766087	624626
Number of scaffolds		247	387	820	239
GC content		45.97%	51.98%	41.19%	49.50%
Total gene count		2059	2022	2997	680
Genome completeness estimate [7]		91.18%	90.38%	88.86%	36.28%
Genome contamination estimate [7]		0.65%	8.20%	2.58%	0.16%
Strain heterogeneity [7]		0.00%	66.67%	25.00%	0.00%
Proportion of sequence reads		4.3471%	1.2903%	4.0885%	0.1088%
GOLD Analysis Project Id	Ga0401162	Ga0401164	Ga0401864	Ga0401165	Ga0401166
IMG Submission ID	221621	221617	222469	221619	221620
GenBank accession number		PYCK00000000	PYCL00000000	JAABVG000000000	JAABVH000000000

Supplementary Table 4. FISH-nanoSIMS analysis of ANME-SRB consortia at single-cell level with different electron acceptors.

Electron acceptor condition	Number of cell ROIs analyzed	ANME-2a ^{15}N atom percent	ANME-2c ^{15}N atom percent	SRB ^{15}N atom percent
Sulfate	525	1.42 ± 0.39% (n=219)	1.60 ± 0.46 (n=27)	1.97 ± 0.68 (n=279)
AQDS	2885	0.70 ± 0.43 (n=980)	0.80 ± 0.36 (n=516)	0.42 ± 0.12 (n=1389)
AQDS+Sulfate	3567	1.49 ± 0.45 (n=1204)	1.09 ± 0.33 (n=552)	0.52 ± 0.29 (n=1810)
None	1238	0.38 ± 0.02 (n=545)	0.38 ± 0.0002 (n=130)	0.37 ± 0.03 (n=563)

Supplementary Table 5. FISH-nanoSIMS analysis of ANME-SRB consortia at single-consortium level with different electron acceptors. The mean of the cell ROIs in a consortium was used for the calculation.

Electron acceptor condition	Number of consortia analyzed	ANME-2a ^{15}N atom percent	ANME-2c ^{15}N atom percent	SRB ^{15}N atom percent
Sulfate	7	1.55 ± 0.41 (n=5)	1.61 ± 0.40 (n=2)	2.17 ± 0.87 (n=7)
AQDS	29	0.67 ± 0.36 (n=17)	0.88 ± 0.38 (n=12)	0.43 ± 0.09 (n=29)
AQDS+Sulfate	33	1.50 ± 0.32 (n=18)	1.15 ± 0.32 (n=15)	0.55 ± 0.18 (n=33)
None	11	0.38 ± 0.02 (n=6)	0.37 ± 0.02 (n=5)	0.38 ± 0.02 (n=11)

Supplementary Table 6. Key pathways in ANME-2a.
(separate table)

Supplementary Table 7. Key pathways in ANME-2c.
(separate table)

Supplementary Table 8. Differential gene expression between AQDS-coupled and sulfate-coupled AOM.
(separate table)

Supplementary Table 9. Differential gene expression during AQDS-coupled AOM with or without sulfate amendment.
(separate table)

References in Supplementary Information

1. Orphan VJ, Hinrichs K-U, Ussler W, Paull CK, Taylor LT, Sylva SP, et al. Comparative Analysis of Methane-Oxidizing Archaea and Sulfate-Reducing Bacteria in Anoxic Marine Sediments. *Appl Environ Microbiol* 2001; **67**: 1922–1934.
2. Waite DW, Chuvochina M, Pelikan C, Parks DH, Yilmaz P, Wagner M, et al. Proposal to reclassify the proteobacterial classes *Deltaproteobacteria* and *Oligoflexia*, and the phylum *Thermodesulfobacteria* into four phyla reflecting major functional capabilities. *Int J Syst Evol* 2020.
3. Skennerton CT, Chourey K, Iyer R, Hettich RL, Tyson GW, Orphan VJ. Methane-fueled syntrophy through extracellular electron transfer: uncovering the genomic traits conserved within diverse bacterial partners of anaerobic methanotrophic archaea. *mBio* 2017; **8**: e00530–e00517.
4. Krukenberg V, Riedel D, Gruber Vodicka HR, Buttigieg PL, Tegetmeyer HE, Boetius A, et al. Gene expression and ultrastructure of meso- and thermophilic methanotrophic consortia. *Environ Microbiol* 2018.
5. Wang F-P, Zhang Y, Chen Y, He Y, Qi J, Hinrichs K-U, et al. Methanotrophic archaea possessing diverging methane-oxidizing and electron-transporting pathways. *ISME J* 2014; **8**: 1069–1078.
6. Milucka J, Ferdelman TG, Polerecky L, Franzke D, Wegener G, Schmid M, et al. Zero-valent sulphur is a key intermediate in marine methane oxidation. *Nature* 2012; **491**: 541–546.
7. Parks DH, Imelfort M, Skennerton CT, Hugenholtz P, Tyson GW. CheckM: assessing the quality of microbial genomes recovered from isolates, single cells, and metagenomes. *Genome Res* 2015; **25**: 1043–1055.